Available online at www.sciencedirect.com
SCIENCE DIRECT
Chemical Physics Letters 421 (2006) 179–183
CHEMICAL PHYSICS LETTERS
www.elsevier.com/locate/cplett

A mechanistic study of H_2S decomposition on Ni- and Cu-based anode surfaces in a solid oxide fuel cell

Y.M. Choi [a], Charles Compson [a], M.C. Lin [b], Meilin Liu [a,*]

[a] Center for Innovative Fuel Cell and Battery Technologies, School of Materials Science and Engineering, 771 Ferst Drive, N.W. Georgia Institute of Technology, 0245 Atlanta, GA 30332, United States
[b] Department of Chemistry, Emory University, 1515 Dickey Drive, Atlanta, GA 30322, United States

Received 8 August 2005; in final form 6 January 2006
Available online 10 February 2006

Abstract

The mechanisms of interaction between H_2S and Ni- or Cu-based anode surfaces in a solid oxide fuel cell were elucidated by density functional slab model calculations. Two reaction pathways via molecular and dissociative adsorption processes were mapped out following minimum energy paths. The energy for H_2S adsorption at the atop site of Ni(1 1 1) lying parallel to the surface is predicted to be -0.55 eV, while that for the dissociative adsorption is -1.75 eV. In contrast, the formation of initial molecular complexes on a Cu surface is energetically unfavorable ($E_{ad} \sim 0.0$ eV), suggesting that Cu is more sulfur-tolerant than Ni.

1. Introduction

One unique advantage of solid oxide fuel cells (SOFCs) over other types of fuel cells is the potential for direct utilization of a wide range of fuels, including natural gas, liquid fuels, gasified coal, and biofuels [1–3]. Many of these fuels, however, come with contaminants such as sulfur-containing compounds, which are difficult to remove economically below ppm level and greatly degrade fuel cell performance. Thus, it is imperative to develop novel anode materials for SOFCs that can tolerate low concentration of sulfur contaminants. While Cu-based anode materials have been extensively studied due to their better sulfur tolerance than Ni-based anodes [1,2], little high level computations have been performed [4]. Recently, a direct comparison of sulfur tolerance on Ni and Cu surfaces in terms of adsorption energies at the same level of periodic density functional theory (DFT) was reported [5]. A reliable mechanistic study for hydrogen sulfide (H_2S) decomposition on the anode surfaces at the molecular level may increase the understanding of incipient sulfur formation, which can be applied to guide the development of new sulfur-tolerant materials. In this study, we report the mechanisms of interaction between H_2S and the most densely packed Ni and Cu{1 1 1} surfaces using periodic DFT calculations. In addition, we have estimated vibrational frequencies with various optimized structures of adsorbed H_2S and HS, together with the detailed potential energy surfaces for all low-lying reaction pathways from H_2S to S.

2. Computational methods

Electronic structure calculations by solving the Kohn–Sham equations were performed using the VASP (Vienna ab initio simulation package) software [6,7] with the projected augmented wave method (PAW) [8]. Surface models were constructed with periodic boundary conditions to mimic infinite surfaces. Generalized gradient approximation (GGA) using the Perdew–Wang (PW91) functional [9] was utilized to describe the exchange and correlation energies. The Brillouin zone was sampled at $(5 \times 5 \times 1)$ k-point with the Monkhorst–Pack method [10]. A kinetic energy cut-off of 400 eV was used for all the calculations. The second order Methfessel–Paxton method [11] was used for the Fermi surface smearing with a 0.2 eV width. In this

* Corresponding author. Fax: +1 404 894 9140.
E-mail address: meilin.liu@mse.gatech.edu (M. Liu).

0009-2614/$ - see front matter © 2006 Elsevier B.V. All rights reserved.
doi:10.1016/j.cplett.2006.01.059

study, all slabs were separated by a vacuum spacing greater than 10 Å. As described in our previous work [5], a five-layer supercell model was constructed. Each layer of this model has four atoms to represent a $p(2\times2)$ unit cell that corresponds to a surface coverage of 0.25 monolayer (ML). The calculations were first carried out by fixing all layers to locate stable intermediates and then by relaxing the three uppermost layers to re-optimize energetically favorable intermediates for mechanistic studies. All the unrelaxed layers were set to estimated bulk parameters. Moreover, vibrational frequencies were calculated, providing a scientific basis for investigations into sulfur-tolerant anode materials using vibrational spectroscopy [5]. In addition to the periodic DFT method, the structures and vibrational frequencies of gas-phase H_2S and HS were calculated by using the PW91PW91/6-31+G(d) level of theory as employed in the GAUSSIAN 03 package [12]. In this study, we calculated the relative energies according to the following equation.

$$\Delta E = E[\text{slab} + \text{adsorbate}] - E[\text{slab}] - E[\text{adsorbate}]$$

where E[slab + adsorbate], E[slab], E[adsorbate] are the calculated electronic energies of adsorbed species on a metal surface, a bare metal surface, and a gas-phase molecule. It should be noted that all surface calculations were carried out with non-spin-polarization methods since the magnetic effect for Ni(1 1 1) using spin-polarization calculations is insignificant for adsorption energies and geometries [13,14].

3. Results and discussion

3.1. Calculations of bulk Ni(1 1 1) and Cu(1 1 1) surfaces and gas-phase H_2S and HS

Estimated bulk lattice constants for Ni(1 1 1) and Cu(1 1 1) are 3.53 and 3.64 Å, respectively, which are in close agreement with the experimental values of 3.52 and 3.61 Å [15]. The optimal Ni–Ni bond distance varies from 2.453 to 2.477 Å, while that of Cu–Cu varies from 2.542 to 2.568 Å. Changing the pseudopotentials from GGA-PAW to ultrasoft pseudopotentials has no effect on the lattice constants. As summarized in Table 1, predicted geometrical parameters and vibrational frequencies of gas-phase H_2S and HS in a 10 Å cubic box are in line with available experimental and theoretical data.

3.2. Reaction mechanisms

The decomposition of H_2S on a metallic anode surface (M) may proceed by stepwise molecular and dissociative adsorptions according to the following scheme.

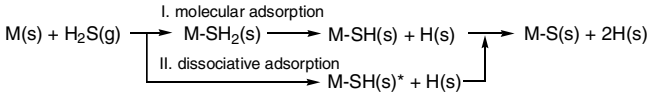

where, s, g, and asterisk stand for surface, gas, and a different adsorbed intermediate.

Table 1
Geometrical parameters and vibrational frequencies of gas-phase H_2S and HS calculated at the GGA–PAW method

Symmetry	H_2S		HS	
	C_{2v}		$C_{\infty v}$	
	Calc[a]	Experiment[b]	Calc[a]	Experiment[c]
r(S–H) (Å)	1.350 [1.357]	1.328	1.355 [1.363]	1.345
θ(H–S–H) (°)	92.1 [92.3]	91.6		
υ_{asym} (cm^{-1})	2669 [2660]	2628	2612 [2622]	2660
υ_{sym} (cm^{-1})	2658 [2636]	2615		
υ_{bend} (cm^{-1})	1226 [1207]	1183		

[a] Values in brackets were predicted at the PW91PW91/6-31+G(d) level of theory using the GAUSSIAN 03 code [12].
[b] From Ref. [16].
[c] From Ref. [17].

3.2.1. Molecular adsorption

In order to initially locate favorable geometries of various species, calculations were performed on an unrelaxed Ni surface, in which only adsorbed H_2S species were fully optimized. An H_2S molecule was placed on four active sites, i.e., atop, bridge, and threefold hcp and fcc [5], producing four types of local intermediates as shown in Fig. 1.

Table 2 lists adsorption energies and molecular parameters of adsorbed H_2S species on the Ni(1 1 1) surface. The atop-site **matop-parallel** lying parallel to the surface is the most stable with an adsorption energy of −0.48 eV on the unrelaxed surface similar to the interactions of H_2S–Pd(1 1 1) [18] and H_2O–Cu(1 1 1) [19], while **matop-up** with the sulfur atom toward the surface is weakly bound with an adsorption energy of −0.14 eV. The bridge-site **mabrg** minimum is also stable with an adsorption energy of −0.42 eV. Interestingly, an initial geometry optimization with a parallel orientation at the bridge site produces the dissociative **dabrg** species that will be discussed in the following section. The **mahcp** and **mafcc** intermediates on

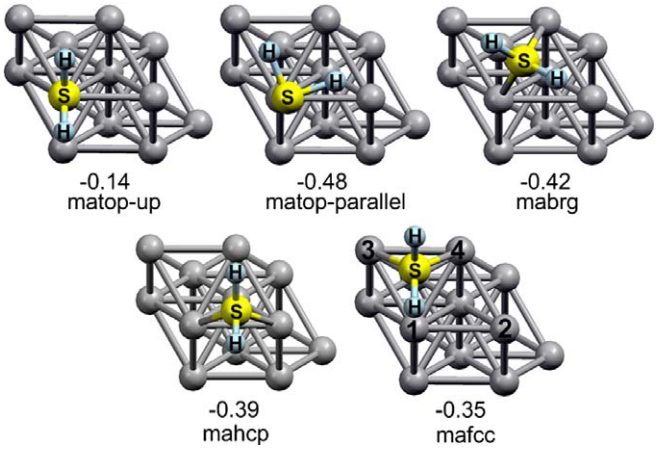

Fig. 1. Schematic illustration of intermediates for the molecular adsorption optimized on four active sites, i.e., atop, bridge, and threefold hcp and fcc. The values are for calculated adsorption energies in eV on the unrelaxed surface. Ni, S, and H atoms are in gray, yellow, and light blue, respectively (For interpretation of the references in colour in this figure legend, the reader is referred to the web version of this article).

Table 2
Adsorption energies and molecular parameters, i.e., bond length in (Å) and angle in (°), of adsorbed H_2S species on Ni(1 1 1)

Active site	atop		bridge[b]	hcp	fcc
Species	**matop-up**	**matop-parallel**	**mabrg**	**mahcp**	**mafcc**
E_{ad}[a]	−0.14	−0.48 [−0.55]	−0.42 [−0.48]	−0.39	−0.35
r(S–H)	1.361	1.375 [1.367]	1.370 [1.373]	1.370	1.385
	1.359	1.374 [1.371]	1.374 [1.375]	1.375	1.370
θ(H–S–H)	95.0	91.6 [91.3]	92.0 [93.7]	91.5	89.8
d(s–S)[c]	2.222	2.182 [2.170]	1.828 [1.753]	1.777	1.793
γ(Ni–H–S–H)	179.0	101.5 [102.4]	138.3 [136.6][d]	138.9[d]	141.4[d]
			135.4 [134.2][e]	141.2[f]	141.4[g]

[a] Adsorption energies in eV relative to unrelaxed or relaxed Ni(1 1 1) and a gas-phase H_2S molecule.
[b] In brackets, the adsorption energy and parameters were calculated on relaxed Ni(1 1 1), otherwise on unrelaxed Ni(1 1 1).
[c] Vertical distance between surface and sulfur atom.
[d–g] $\gamma(Ni_1–H–S–H)\gamma(Ni_4–H–S–H)$, and $\gamma(Ni_2–H–S–H)$, respectively, are dihedral angles. (see **mafcc** in Fig. 1 for numbering).

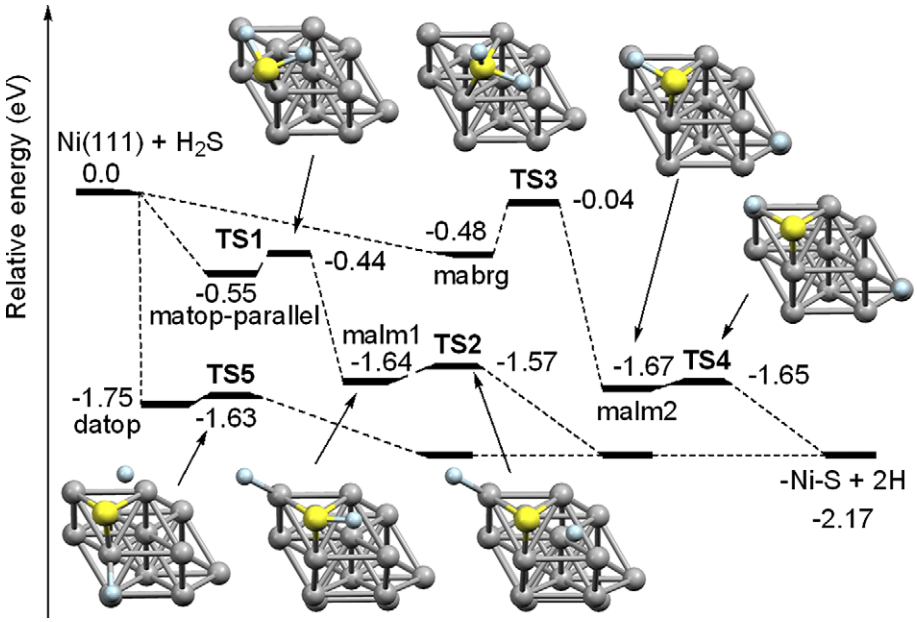

Fig. 2. Schematic energy profiles for H_2S–Ni(1 1 1) interactions via the molecular and dissociative adsorption on the surface by relaxing the three uppermost layers. Relative energies are in eV.

threefold hcp and fcc sites, respectively, have adsorption energies of −0.39 and −0.35 eV, respectively. Their sulfur atoms are insignificantly shifted from the center Ni atoms (see Fig. 1). The atop-site **matop-parallel** and bridge-site **mabrg** intermediates, summarized in Table 2, are applied for a mechanistic study of the molecular adsorption since they are energetically the most favorable. All surface calculations for the mechanistic study were carried out on the surface by relaxing the three uppermost layers as mentioned before. For the molecular adsorption pathway shown in Fig. 2, the first step is the barrierless formation of the molecular precursor **matop-parallel** and **mabrg** with exothermicities of 0.55 and 0.48 eV, respectively. These values are close to the exothermicities of the H_2S molecular complex on pyrite (FeS_2) [20], Fe(1 0 0) [21], and Fe(1 1 0) [22] (0.48, 0.46, and 0.50 eV, respectively), but are slightly different from that on Pd(1 1 1) with a 0.22 ML coverage (0.66 eV) [18].

For a reaction pathway via the **matop-parallel** intermediate, it produces **malm1**, –Ni–SH + H, with the exothermicty of 1.64 eV after overcoming a reaction barrier of 0.07 eV via **TS1**, while the adsorbed sulfide on **mabrg** can decompose via **TS3** lying 0.04 eV below the reactants (or 0.44 eV above **mabrg**) to give **malm2** with the exothermicity of 1.67 eV, assuming the H atoms are totally dissociated. The **malm1** and **malm2** intermediates can further fragment to give –Ni–S + 2H with an exothermicity of 2.17 eV after overcoming a small reaction barrier of **TS2** and **TS4**, respectively. Then, a dissociated hydrogen atom diffuses on the surface. In this study, we restricted optimization processes within the Ni(1 1 1) supercell model to avoid any unnecessary interactions. To have a better picture of the surface and the distances between atoms in the neighboring cells, we depict a larger surface fragment corresponding to a $p(4 \times 4)$ unit cell with final products, –Ni–S + 2H. (see Fig. 3) A short distance found between

H atoms in neighboring cells, 1.796 Å (1.492 Å for the dissociative pathway), may be indicative of a further H_2 forming process under fuel-cell operating conditions. In addition, we examined the effect of surface coverage on adsorption energies. For the calculations, unrelaxed three-layer surface model similar to Alfonso and coworkers [18] was used to save CPU resources. For the atop site **matop-parallel** intermediate, decreasing the coverage from 0.25 to 0.11 ML corresponding to $p(2\times2)$ and $p(3\times3)$ super cells, respectively, leads to a slight change in adsorption energy from −0.58 and −0.62 eV (∼8%). The surface coverage effects on energetics for other local minima, and transition states will be reported in subsequent communications. Under fuel-cell operating conditions, we assume the surface products may further react with oxygen anion (O^{2-}) forming H_2O and SO_2 or interact with each other producing H_2 molecules via the apparently short hydrogen bond. Furthermore, the adsorbed sulfur atom may diffuse to the other active sites, i.e., atop, bridge, and hcp, as described elsewhere [5].

It is interesting to note that the predicted adsorption energies for the molecular adsorption of H_2S on an unrelaxed Cu(1 1 1) surface at atop, bridge, and threefold hcp and fcc sites are −0.04 and −0.09, −0.02, 0.00, 0.01 eV, respectively, supporting mechanistically the fact that Cu-based anodes are more sulfur-tolerant as mentioned in Section 1. Their energetics and geometrical parameters are compiled in Table 3.

3.2.2. Dissociative adsorption

Similar to the molecular adsorption process, an initial geometry was optimized on the unrelaxed Ni surface by placing a hydrogen atom on the atop site as shown in Fig. 4, producing not a molecularly adsorbed intermediate but a dissociated intermediate in decomposed HS and H. In addition to the atop site, the two hydrogen atoms of the H_2S molecule were located on atop-to-atop (Ni_1–Ni_4) and hcp-to-fcc, resulting in **dabrg** and **dahcp-fcc**, respectively. Their energetics and geometrical data are summarized in Table 4. Similar to the molecular adsorption, we re-optimized **datop**, due to its highest stability, by relaxing the three uppermost layers to carry out a mechanistic study for the dissociative adsorption. Shown in Fig. 2 is a potential energy profile for the dissociative adsorption on the Ni(1 1 1) surface. As an H_2S molecule without a barrier approaches the Ni surface presented, the total energy

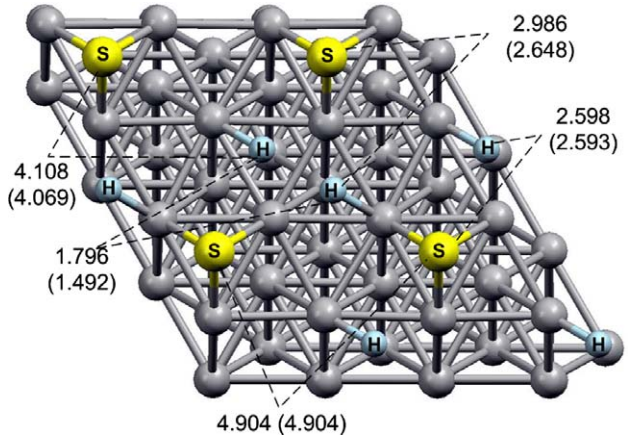

Fig. 3. Geometrical illustration of surface adsorbed products on Ni(1 1 1) via the molecular and dissociative adsorption. Given in parentheses are the bond distances of the final products for the dissociative adsorption. Bond lengths are in Å.

Table 3
Adsorption energies and molecular parameters, i.e., bond length in (Å) and angle in (°), of adsorbed H_2S species on Cu(1 1 1) without surface relaxation

Active site	atop		bridge	hcp	fcc
	up	parallel			
E_{ad}[a]	−0.04	−0.09	−0.02	0.00	0.01
r(S–H)	1.353 1.352	1.352 1.351	1.358 1.355	1.361 1.355	1.360 1.353
θ(H–S–H)	92.1	91.7	93.6	92.3	94.2
d(s–S)[b]	3.402	3.408	3.010	2.799	2.698
γ(Ni–H–S–H)	180.0	92.6	151.3[c] 148.1[d]	132.8[c] 153.8[e]	130.8[c] 161.1[f]

[a] Adsorption energies in eV relative to unrelaxed Cu(1 1 1) and a gas-phase H_2S molecule.
[b] Vertical distance between surface and sulfur atom.
[c–f] $\gamma(Cu_1–H–S–H)$, $\gamma(Cu_4–H–S–H)$, $\gamma(Cu_2–H–S–H)$, and $\gamma(Cu_3–H–S–H)$, respectively, are dihedral angles.

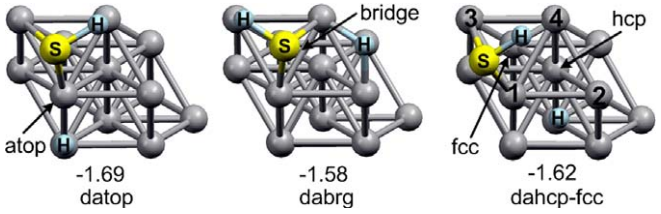

Fig. 4. Schematic illustration of intermediates for the dissociative adsorption optimized on three active sites, i.e., atop, atop-to-atop, and hcp-to-fcc, respectively. The values are calculated adsorption energies in eV. Ni, S, and H atoms are in gray, yellow, and pale blue, respectively (For interpretation of the references in colour in this figure legend, the reader is referred to the web version of this article).

Table 4
Adsorption energies and molecular parameters, i.e., bond length in (Å) and angle in (°), of adsorbed HS species on Ni(1 1 1) via the dissociative adsorption

Active site	atop[b]	bridge	hcp-fcc
Species	**datop**	**dabrg**	**dahcp-fcc**
E_{ad}[a]	−1.69 [−1.75]	−1.58	−1.62
r(S–H)	1.412 [1.416]	1.400	1.370
θ(Ni–S–Ni)	68.5 [69.3]	67.3	56.4
d(s–S)[c]	1.747 [1.738]	1.778	1.784
γ(Ni–Ni–S–H)[d]	102.2 [100.6]	105.5	102.7

[a] Adsorption energies in eV relative to unrelaxed or relaxed Ni(1 1 1) and a gas-phase H_2S molecule.
[b] The adsorption energy and parameters in brackets were calculated on relaxed Ni(1 1 1).
[c] Vertical distance between surface and sulfur atom.
[d] Dihedral angle.

Table 5
Calculated vibrational frequencies[a] in cm^{-1} of adsorbed H_2S and HS species for the molecular and dissociative adsorptions on Ni(1 1 1)

Molecular adsorption[b]						Dissociative adsorption[c]		
v_i	**matop-up**	**matop-parallel**	**mabrg**	**mahcp**	**mafcc**	**datop**	**dabrg**	**dahcp-fcc**
v_1	2516	2388 [2426]	2390 [2372]	2398	2387	2110 [2057]	2210	2298
v_2	2499	2355 [2380]	2343 [2339]	2312	2252	1234 [1238]	1245	1283
v_3	1153	1082 [1093]	1143 [1135]	1149	1173			

[a] The vibrational modes in brackets were calculated on relaxed Ni(1 1 1), otherwise on the unrelaxed Ni(1 1 1) surface.
[b] v_1 and v_2 and v_3 correspond to two S–H stretching and H–S–H bending modes, respectively.
[c] v_1 and v_2 correspond to S–H and Ni–H stretching modes, respectively.

decreases, forming **datop** with an exothermicity of 1.75 eV. After overcoming **TS5** with a small 0.12 eV barrier, the H atom of the surface HS species dissociates, producing similar products as in the case of molecular adsorption (see Fig. 3), in which a sulfur atom is located on the fcc site. The exothermicity of the final products is the same as that of the molecular adsorption. Similar to the molecular adsorption, a further H_2 forming process can occur through the dissociative adsorption due to the short H–H bond distance of 1.492 Å (see Fig. 3).

In addition to the mechanistic studies, as summarized in Table 5, to guide surface vibrational spectroscopy, the vibrational frequencies for the adsorbed H_2S and HS species on the Ni(1 1 1) surfaces were estimated by displacing adsorbed species. Since the adsorbed sulfur atoms are strongly bound to the surface, predicted vibrational frequencies for the surface-S stretching mode may be close to that of a sulfur atom solely adsorbed at the fcc site of Ni(1 1 1) (441 cm^{-1}) [5].

4. Conclusion

The interactions of H_2S with Ni- and Cu-based anodes for SOFCs have been examined by periodic DFT calculations to elucidate the reaction mechanisms of H_2S adsorption and decompostion. Two reaction pathways via molecular and dissociative adsorption were studied based on energetically favorable species. Comparing adsorption energies of adsorbed H_2S sepcies on Ni(1 1 1) and Cu(1 1 1), Cu is much more surfur-tolerant than Ni due to its weak binding energy ($E_{ad} \sim 0.0$ eV), implying no further interaction on the Cu surface. We plan to examine the further interations of the dissocatied hydrogen and/or sulfur atoms with oxygen ions (O^{2-}) electrochemically pumped through an electrolyte such as yittria-doped zirconia or gadolia-doped ceria under fuel-cell operating conditions.

Acknowledgements

The authors are grateful for the financial support of this work provided by DOE-NETL-SECA core technology program (Grant No. DE-FC26-04NT42219) directed by Dr. Lane Wilson. The authors also appreciate the reviewer's critical comments that made the manuscript more meaningful and informative. We acknowledge the use of CPU's from National Center for High-performance Computing, Taiwan. MCL acknowledges the support from Taiwan National Science Council for a Distinguished Visiting Professorship at the Center for Interdisciplinary Molecular Science, Chiao Tung University, Hsinchu, Taiwan.

References

[1] H. Kim, J.M. Vohs, R.J. Gorte, Chem. Commun. (2001) 2334.
[2] L.G. Marianowski, G.L. Anderson, E.H. Camara, US Patent 5 071 718 (1988).
[3] L. Aguilar, S. Zha, Z. Cheng, J. Winnick, M. Liu, J. Power Source 135 (2004) 17.
[4] S.P. Walch, W.A. Goddard III, Surf. Sci. 72 (1978) 645.
[5] Y.M. Choi, C. Compson, M.C. Lin, M. Liu, J. Solid State Chem., submitted for publication.
[6] G. Kresse, J. Furthmüller, Phys. Rev. B 54 (1996) 11169.
[7] G. Kresse, J. Hafner, Phys. Rev. B 47 (1993) 558.
[8] P. Blochl, Phys. Rev. B 17 (1994) 953.
[9] J.P. Perdew, Y. Wang, Phys. Rev. B 45 (1992) 13244.
[10] H.J. Monkhorst, J.D. Pack, Phys. Rev. B 13 (1976) 5188.
[11] M. Methfessel, A.T. Paxton, Phys. Rev. B 40 (1989) 3616.
[12] M.J. Frisch et al., GAUSSIAN 03, Revision C.01, Gaussian Inc., Wallingford, CT, 2004.
[13] G. Kresse, J. Hafner, Surf. Sci. 459 (2000) 287.
[14] F. Mittendorfer, J. Hafner, Surf. Sci. 472 (2001) 133.
[15] CRC Handbook of Chemistry and Physics, CRC Press, New York, 1996.
[16] G. Herzberg, Molecular Spectra and Molecular StructureElectronic Spectra and Electronic Structure of Polyatomic Molecules, vol. III, Krieger, Malabar, FL, 1966.
[17] K.P. Huber, G. Herzberg, Molecular Spectra and Molecular StructureConstants of Diatomic Molecules, vol. IV, Van Nostrand, New York, 1979.
[18] D.R. Alfonso, A.V. Cuginia, D.C. Sorescua, Catal. Today 99 (2005) 315.
[19] H. Ruuska, T.A. Pakkanen, R.L. Rowley, J. Phys. Chem. B 108 (2004) 2614.
[20] A. Stirling, M. Bernasconi, M. Parrinello, J. Chem. Phys. 119 (2003) 4934.
[21] D.E. Jiang, E.A. Carter, J. Phys. Chem. B 108 (2004) 19140.
[22] D.E. Jiang, E.A. Cater, Surf. Sci. 583 (2005) 60.